THE ASTROPHYSICAL JOURNAL, 489:199–209, 1997 November 1

TIME-DEPENDENT ACCRETION BY MAGNETIC YOUNG STELLAR OBJECTS AS A LAUNCHING MECHANISM FOR STELLAR JETS

ANTHONY P. GOODSON
Physics Department, University of Washington, Seattle, WA 98195; anthony@geophys.washington.edu
ROBERT M. WINGLEE
Geophysics Program, University of Washington, Seattle, WA 98195; winglee@geophys.washington.edu
AND
KARL-HEINZ BÖHM
Astronomy Department, University of Washington, Seattle, WA 98195; bohm@astro.washington.edu
Received 1997 February 21; accepted 1997 June 10

ABSTRACT

A time-dependent jet launching and collimating mechanism is presented. Initial results of numerical simulations of the interaction between an aligned dipole rotator and a conducting circumstellar accretion disk that is initially threaded by the dipole field show that differential rotation between the disk and the star leads to the rapid expansion of the magnetic loops that connect the star to the disk. The expansion of these magnetic loops above and below the disk produces a two-component outflow. A hot, well-collimated outflow is generated by the convergent flow of attached plasma toward the rotation axis, while a cool, slower outflow is produced on the disk side of the expanding loop. The expanding loop, which later forms a plasmoid, defines the boundary between the jetlike flow and the disk wind. Episodic magnetic reconnection above and below the disk releases the jet plasma from the system and allows the process to repeat, reinforcing the hot, well-collimated outflow.

Subject headings: accretion, accretion disks — ISM: jets and outflows — methods: numerical — MHD — stars: pre–main-sequence

1. INTRODUCTION

Many newly formed stars generate jets of plasma that penetrate the interstellar medium (ISM) for distances as great as parsecs. Herbig-Haro objects were first detected in 1951 (Herbig 1951), although no association with stellar jets was demonstrated at that time. Much later, in the 1980s, it was concluded that Herbig-Haro objects are indicators of stellar jets. It has been demonstrated with some certainty that most of these objects are shock waves around the head of very narrow, very fast streams of plasma (Hartmann & Raymond 1984; Hartigan, Raymond, & Hartmann 1987).

Stellar jets are populous in regions of star formation. New *Hubble Space Telescope* (*HST*) images of the Orion Nebula show literally hundreds of Herbig-Haro objects (O'Dell & Wen 1994). Reipurth (1994) has listed 285 Herbig-Haro objects individually. For most jets, a pre–main-sequence star or an embedded young stellar object (YSO) has been identified as the candidate source (Edwards, Ray, & Mundt 1993). Furthermore, some of these infrared sources have been found to be X-ray sources as well, indicating significant magnetic activity (Feigelson et al. 1993).

Where observable, the systems that generate jets have characteristics of accretion disks. Accretion disk motion has been found in infrared and millimeter wavelength spectral observations of the vicinity of YSOs, and in a few cases accretion disks have been observed optically with the *HST*. Whenever disk/jet systems have been observed, the jet has been found to be perpendicular to the accretion disk (Edwards et al. 1993). Jets are generally found in pairs, and in the cases in which only one jet is found, it is assumed that the other is obscured by the accretion disk (see, e.g., Hirth 1994).

Doppler shift of emissions from jet plasma and jets' proper motions indicate that plasma in stellar jets travels at speeds of 200–400 km s^{-1}. These speeds are approximately consistent with the line profiles and position-velocity diagrams of Herbig-Haro objects (Herbig 1981; Eisloeffel, Mundt, & Böhm 1994; Raga & Böhm 1986; Hartigan et al. 1987). Jets have "knots," bright regions that move along with the jet. It was originally thought that these knots were stationary "crossing shocks," a supersonic nozzle phenomenon. Calculations have shown that the spacing between—and the proper motions of—these knots are inconsistent with this view (Raga 1989). Recent *HST* observations, which show the knots more as a "ticker tape," suggest that these knots may really be a series of "interstellar bullets" of hot plasma. This implies that the jet may really be not a stream of material but a chain of these bullets (see, e.g., Raga & Kofman 1992).

Recent *HST* imaging observations and spectroscopic observations using Solf's method show that jets are highly collimated in a very short distance (Solf 1989; Ray et al. 1996; Kepner et al. 1993; Böhm & Solf 1994; Hirth, Mundt, & Solf 1994). Observations have shown that the material is collimated within 50 AU of the source star. Should the jet prove to be a series of interstellar bullets, these observations imply that these bullets have a relatively small diameter (at most a few tens of AU) and are launched in the same direction (Mundt 1985; Reipurth 1991). Interestingly, Ray et al. (1996) have shown that if the jets are launched from within a few stellar radii of the star, then the initial opening angle of the jet must be rather large, since the jet has a width of the order of tens of AU when it is only tens of AU from the source. After reaching this distance, the jet becomes fully collimated. At large scales, jets are often accompanied by a poorly collimated, cooler, slower outflow, which is mostly observed in CO (Fukui et al. 1993).

For the region very close to the source star, Kwan &

Tademaru (1988) argue that two separate outflow components contribute to the total observed line emission: a fast, high-speed, well-collimated flow (the jet), and a slower, more poorly collimated outflow, often called a disk wind. This model is supported by the results of the application of Solf's method to spectroscopic observations of outflows from classical T Tauri stars (see, e.g., Solf & Böhm 1993; Böhm & Solf 1994). These results can be interpreted as showing, in addition to the well-collimated jet, a much slower and more poorly collimated component of flow. This slower flow has the following typical properties: (1) The velocity dispersion of the slower flow is comparable to its Doppler velocity, implying poor collimation. (2) The emission peak of the slower component is close to the star (less than 0".5 for DG Tauri). (3) The velocity of the slow component is considerably less than 100 km s^{-1} (55 km s^{-1} for DG Tauri and about 10 km s^{-1} for T Tauri).

It is generally believed that stars that generate jets have strong magnetic fields. X-ray observations of embedded IR sources indicate significant flare-type activity (Koyama et al. 1994), and the magnetic fields of some T Tauri stars have been estimated, using spectra, to be in the 1–2 kG range (Guenther 1997). The first direct evidence for magnetic fields in outflows has recently been found (Ray et al. 1997). Radio observations are interpreted as showing magnetic fields as strong as a few gauss at distances as large as 50 AU from the source star T Tauri South (the infrared companion to T Tauri).

Theoretical efforts toward the understanding of stellar jets have typically focused either on the collimation mechanism or on the launching mechanism. Both hydrodynamic and magnetohydrodynamic (MHD) collimation mechanisms have been studied. Raga & Cantó (1989), expanding on earlier work by Königl (1982), examined collimation via a de Laval nozzle (which would be formed by the inertial confinement produced by the surrounding molecular cloud), finding that collimation is possible, but not on the length scales observed. Frank & Mellema (1996) have recently reexamined hydrodynamic collimation and found it to be possible via shock focusing. Magnetic collimation via a centrifugal wind has been investigated extensively and found to be plausible (see, e.g., Königl & Ruden 1993).

With the major exception of the work of Uchida & Shibata (Uchida & Shibata 1985; Shibata & Uchida 1986), most theoretical efforts at addressing the jet launching mechanism have assumed that jets are steady (Shu et al. 1994a, 1994b; Najita & Shu 1994). Observational evidence, however, has pointed more toward an unsteady jet launching mechanism (see, e.g., Cameron & Liseau 1990; Ray et al. 1996). Most recently, *HST* observations have implied that jets from YSOs consist of outbursts with timescales on the order of years. There are also theoretical grounds (discussed below) for believing that the jet launching mechanism, as well as accretion by the star, is inherently unsteady.

This paper presents results of time-dependent MHD simulations that produce outflows from star/disk systems that meet most of the constraints imposed by observations. The jet is both launched and collimated by the interaction of the stellar magnetic field with the accretion disk. A two-component outflow arises, consisting of a highly collimated fast, hot jet and a poorly collimated, slow, cool disk wind. The flow is sustained through the process of magnetic reconnection.

Section 2 addresses the basic theory of the jet launching mechanism, building on past work by Ghosh & Lamb (1978, 1979a, 1979b), Zylstra (1988), Lovelace, Romanova, & Bisnovatyi-Kogan (1995), and the time-dependent numerical simulation work of Hayashi, Shibata, & Matsumoto (1996). The details of the method used for the numerical simulation are presented in § 3. Section 4 presents the results of the time-dependent simulation, including the jetlike outflow and its companion disk wind. The implications of the results are laid out in § 5.

2. THEORY

The recent rapid accrual of observational evidence relating to jet formation has led many to believe that the interaction between the source star's magnetic field and the surrounding disk plays an important role. One of the first models to deal with this interaction was the neutron star disk-accretion model of Ghosh & Lamb (1978, 1979a, 1979b). This model, illustrated in Figure 1, is used to address the relationship between accretion rate (or accretion luminosity) and the spin-up/spin-down of the pulsar

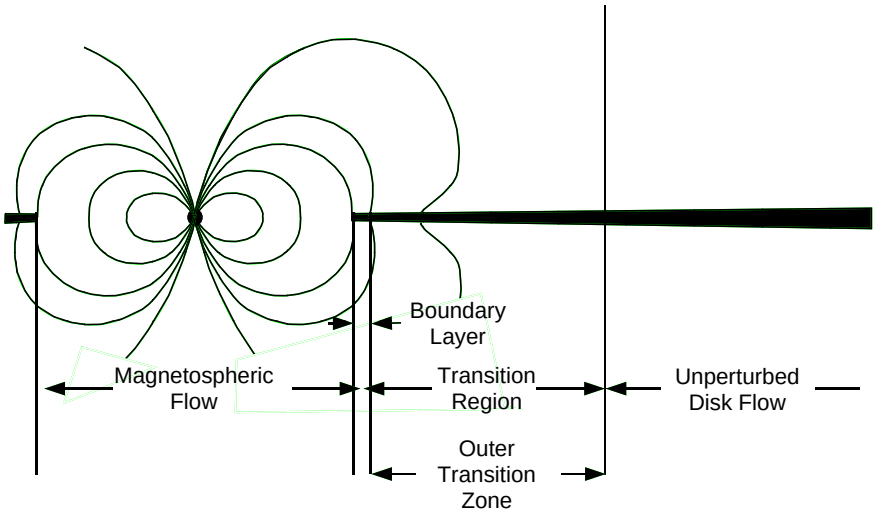

FIG. 1.—Model of Ghosh & Lamb (1978). Magnetic flux from the star threads the disk in the broad outer transition zone. Diffusive instabilities allow field slippage in this region.

and does not address stellar jets. The disk in this model is threaded by the pulsar's magnetic field. Flow in the disk far from the star is dominated by viscous stresses and is essentially Keplerian. At closer radii, magnetic stresses begin to play a role, resulting in a broad transition zone in which the flow ceases to be Keplerian and makes a transition to corotation. Finally, close to the star, the magnetic stresses dominate, the disk is truncated, and plasma flows along magnetic field lines onto the star.

Ghosh & Lamb (1978, 1979a, 1979b) invoke diffusive instabilities in the disk to prevent the field lines that thread the transition zone from continuously wrapping up. This is an important assumption, as will be shown later, and allows the torque on the star to be determined by the location of the corotation point, the point at which the plasma in the disk is in corotation with the star, with respect to the transition zone. Ghosh & Lamb point out that there may be no steady solution to the flow should the frozen-in flux approximation hold in the transition zone.

Lovelace et al. (1995, hereafter LRBK) examined the magnetic accretion model of Ghosh & Lamb under the condition of very high conductivity and predicted that differential rotation between the star and the disk would cause the field connecting the two to become twisted, inducing an azimuthal component and rapidly inflating the poloidal component of the field. This prediction is consistent with the work of Zylstra (1988) and Aly & Kuijpers (1990). The work of LRBK, as well as the work presented here, ignores the issue of how the magnetic field manages to thread the accretion disk initially.

LRBK show that if the star and disk are rotating at different rates and if magnetic diffusion in the disk is comparable to or less than the hydrodynamic viscosity, then the magnetic field lines will be wrapped up. This wrapping of the field induces an azimuthal component, B_ϕ. The induction of an azimuthal field increases the overall magnetic energy density. Given that the plasma above the disk is thin but conducting, the excess magnetic energy density (or magnetic pressure) will work to "puff out" the field lines connecting the star to the disk. This is illustrated in Figure 2. If the plasma above and below the disk is sufficiently thin and cold so that the Alfvén speed $B/(4\pi\rho)^{0.5}$ is much greater than the sound speed, the expansion can be thought of as an evolution through a series of force-free configurations, each with higher energy than its predecessor.

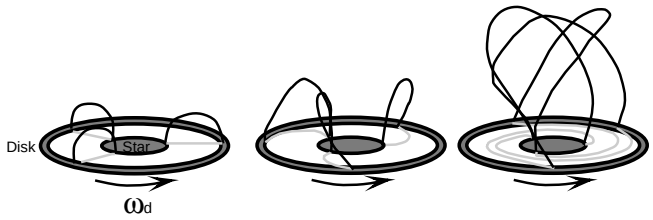

FIG. 2.—After LRBK; poloidal field that initially connects the star to a region of the accretion disk that is rotating at a different rate is wrapped up, inducing a B_ϕ component that increases the total B field. This increase in magnetic energy density causes the loops that connect the star to the disk to inflate rapidly.

LRBK predict that the rapid expansion of poloidal field leads to three field regions close to the star: a closed stellar magnetosphere, a region of effectively open field that connects to the poles of the star, and a region of effectively open field that threads the disk (see Fig. 3). While the open-field lines that thread the disk may actually connect to the star via a very long and extended loop (if the system is in isolation and only a finite amount of evolution has occurred), they may be thought of as effectively open in that it is difficult to transfer magnetic stresses from the star to the disk, and disk plasma has no easy magnetic access to the star. LRBK go on to estimate the impact of the field configuration shown in Figure 3 on accretion/torque relations.

LRBK do not describe the transient magnetic field configuration associated with the expansion, but it will be shown in following sections that the expansion process itself drives an outflow. As the loops that connect the star to the disk expand, plasma attached to those loops is driven either

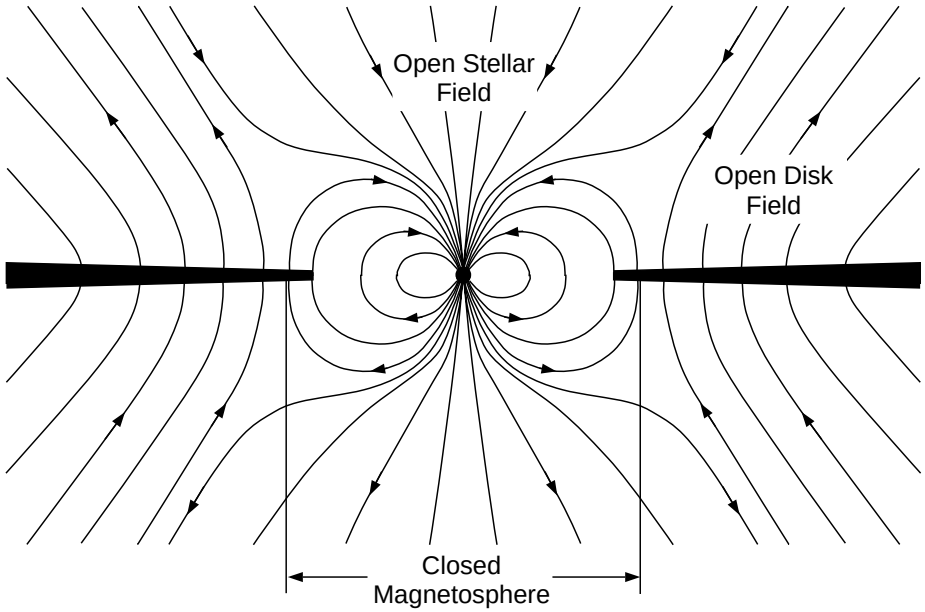

FIG. 3.—Final magnetic field configuration close to the star, as predicted by LRBK. The field has three distinct regions: a closed stellar magnetosphere, an effectively open disk field, and an effectively open stellar field. Note that plasma attached to open disk field lines has no magnetic access to the star.

toward the rotation axis (for plasma on the axis side of the expanding loop) or toward the disk (for plasma on the disk side of the expanding loop). The flow toward the rotation axis is convergent and can produce a collimated outflow, if sustained. Plasma that is flung against the disk is likely to produce a poorly collimated, cool outflow. Plasma that expands outward in the region between the rotation axis and the disk is divergent flow; the density in this region will decrease. Figure 4 illustrates how the rapid expansion of the poloidal field can produce a two-component outflow.

It is shown in following sections that the jet formation process is sustained via magnetic reconnection above and below the accretion disk. Reconnection of the "open" disk field with the "open" stellar field will create a plasmoid (or magnetic island) and will allow the star to be magnetically connected to the differentially rotating disk again. If the footpoint in the disk of these field lines is inside the centrifugal barrier, accretion will be enhanced as disk plasma flows along these field lines and onto the star. Differential rotation between the star and the disk, however, will eventually cause these field lines to expand outward through the process that was described by LRBK. Disk plasma, which is now attached to these field lines, will then be driven either toward the rotation axis to reinforce the jet or toward the disk to form a part of the disk wind.

The field configuration predicted by LRBK also has pertinent implications for accretion. For very high conductivity, the plasma threaded by the open disk field cannot reach the star easily, as it must cross magnetic field lines. Diffusion across field lines at the magnetospheric boundary is the only option for accretion and is invoked by LRBK and similarly by Ghosh & Lamb (1978, 1979a, 1979b). Reconnection above and below the disk, however, will allow the inner edge of the disk to have magnetic access to the star, which would greatly increase the instantaneous accretion rate while simultaneously ejecting the plasmoids from the region above and below the disk. Thus, under the field configuration predicted by LRBK, accretion and mass ejection are modulated by magnetic reconnection. If the conductivity is high at and near the magnetospheric boundary (specifically, if the magnetic diffusivity is less than the effective viscosity of the disk plasma), then plasma flow across magnetic field lines will be inhibited; there may be no steady solution to the accretion flow.

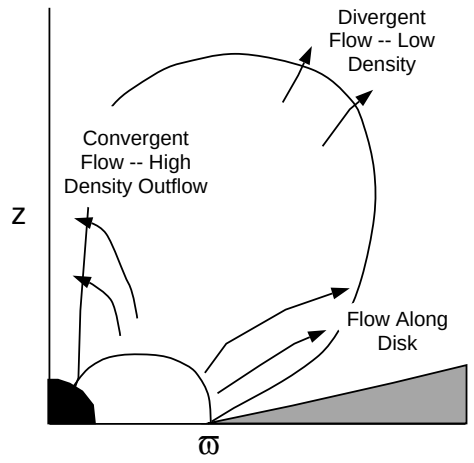

FIG. 4.—Rapid expansion of the poloidal field will drive plasma toward the rotation axis (forming a convergent flow that produces a jet), toward the disk (forming a disk wind), or to the region between (producing a divergent flow with low density).

The recent time-dependent work of Hayashi et al. (1996) has produced the LRBK configuration close to the star. Numerical simulation was used to examine the inflation and reconnection processes in the region close to the star, in an effort to understand the X-ray observations of embedded YSOs (see, e.g., Koyama et al. 1994). It was found that the reconnection event that releases the plasmoids could produce X-ray outbursts that are consistent with observations. The work presented below also produces the LRBK magnetic configuration close to the star, but the simulation size and simulation time are much greater than those of Hayashi et al. (1996), and the early development of a jet and a disk wind is seen.

3. METHOD

To model the flow of disk plasma near the rotating magnetic star, we solve the time-dependent equations of resistive MHD, using the two-step Lax-Wendroff scheme (Richtmyer & Morton 1967). The equations are the continuity equation,

$$\frac{\partial \rho}{\partial t} + \nabla \cdot \rho \boldsymbol{u} = 0 , \tag{1}$$

the momentum equation,

$$\rho \frac{\partial \boldsymbol{u}}{\partial t} + \rho(\boldsymbol{u} \cdot \nabla)\boldsymbol{u} = -\frac{GM_*}{(\bar{\omega}^2 + z^2)} \hat{\boldsymbol{r}} - \nabla P + \frac{1}{c} \boldsymbol{J} \times \boldsymbol{B} , \tag{2}$$

the energy equation,

$$\frac{\partial e}{\partial t} + \nabla \cdot [(e + P)\boldsymbol{u}] = \left[-\frac{GM_*}{(\bar{\omega}^2 + z^2)} \hat{\boldsymbol{r}} \right] \cdot \boldsymbol{u} + \boldsymbol{J} \cdot \boldsymbol{E} , \tag{3}$$

and the induction equation,

$$\frac{\partial \boldsymbol{B}}{\partial t} = -c \nabla \times \boldsymbol{E} , \tag{4}$$

with

$$\boldsymbol{J} = \frac{c}{4\pi} \nabla \times \boldsymbol{B} , \tag{5}$$

$$\boldsymbol{E} = -\frac{1}{c} \boldsymbol{u} \times \boldsymbol{B} + \frac{1}{\sigma} \boldsymbol{J} , \tag{6}$$

and

$$e = \frac{1}{2} \rho |\boldsymbol{u}|^2 + \frac{P}{\gamma - 1} . \tag{7}$$

Here the vectors $\boldsymbol{u}$, $\boldsymbol{B}$, $\boldsymbol{E}$, and $\boldsymbol{J}$ are the velocity, magnetic field, inductive electric field, and current density, respectively. The scalars e, ρ, and P are the internal energy density, mass density, and pressure of the plasma. The second term on the right-hand side of equation (6) allows for finite conductivity (hence resistive MHD). Finite conductivity (or nonzero resistivity) can produce diffusion of the magnetic field in the induction equation and ohmic heating in the energy equation, and can drive magnetic reconnection.

The equations of MHD are derived from fluid mechanics and Maxwell's equations under specific assumptions. Namely, displacement currents (currents associated with

$\partial E/\partial t$) are neglected, and the ion gyroradius is taken to be much smaller than other length scales in the system, such as the mean free path or the thickness of a current sheet.

Axisymmetry is imposed, producing a 2.5-dimensional code. Axisymmetry requires that the rotation axes of the star and disk be aligned with the stellar dipole. This removes the influence of any azimuthal dependence but may simplify the problem to an overidealized case.

The code, which was developed by the authors, was tested for proper behavior across various shock waves as well as for gravitational and rotational dynamics. Furthermore, the implementation of stellar rotation was checked by rotating the magnetized star (with a viscous boundary layer) in a very thin, conducting plasma in order to ensure that the plasma was brought into corotation with the star. The code is similar to a full three-dimensional code used by Elsen & Winglee (1997) to predict the location of the Earth's magnetopause boundary for varying solar wind conditions. (The predictions of this three-dimensional simulation were in some cases as accurate as empirical relations.)

The simulation itself consists of a series of 11 nested boxes. Each box utilizes a grid of 57×49 points, but the grid spacing Δ increases by a factor of 2 between successive boxes. The nesting technique provides for high resolution ($0.1\ R_\odot$) close to the star, while allowing the total simulation area to reach out to large length scales. The largest box is 26 AU wide. This dynamic range in scaling allows the small-scale structure of the magnetosphere/disk interaction to be examined while still capturing the large-scale behavior. The justification for this scheme is that small-scale structure close to the star drives the physics of the launching mechanism, and the jet has large length scales itself at large distances.

The initial conditions have a $1\ M_\odot$ star with a radius of $1.5\ R_\odot$, surrounded by a truncated, conducting accretion disk that is initially threaded by the stellar dipole field. The mechanism by which the disk becomes threaded by this field is not considered. The conductivity is large (but finite) and spatially uniform. Since the conductivity is high enough to allow approximate flux freezing in the disk, the core of the accretion disk in this simulation has a fairly high ionization fraction. Photoionization is not accounted for.

The plasma above and below the disk is described by $\rho = \rho_0/R^4$, where $R = (\bar{\omega}^2 + z^2)^{1/2}$, implying that the initial Alfvén speed outside the disk (V_A) behaves as $V_A = V_{A_0}/R$, where V_{A_0} is the Alfvén speed at the stellar surface (which is latitude dependent). The initial density is chosen so that the Alfvén velocity near the star is 3–4 times the maximum possible infall velocity. The star rotates with a period of 1.8 days.

The accretion disk is taken to be a standard α-model disk (see Frank, King, & Draine 1992) with an accretion rate of $10^{-7}\ M_\odot\ \mathrm{yr}^{-1}$ and $\alpha = 10^{-3}$ close to the star; α has a weak r dependence, such that the peak disk density falls off as $\bar{\omega}^{-13/8}$. The disk is truncated at $8.5\ R_\odot$. The peak stellar surface magnetic field is 1000 G.

4. RESULTS

The results at early times in the system's evolution are qualitatively similar to the results of Hayashi et al. (1996) and the predictions of LRBK for the region close to the star. Figure 5 shows the initial expansion of the magnetic field near the star. The results of this figure can be compared with Hayashi et al. (1996). The initial conditions, with the dipole field threading the accretion disk, are shown in the first panels. The top panels show magnetic field lines, velocity vectors, and temperature (gray scale), while the bottom panels show field lines and $\log_{10}\ \rho$ in gray scale, with 4 orders of magnitude variation in ρ plotted. The bottom row has 4 times the resolution of the top row.

Differential rotation between the star and the region of the disk to which it is magnetically connected induces an azimuthal component of the magnetic field. This azimuthal component is not shown in the figure, but it causes the overall magnetic energy density to increase in the regions above and below the disk. As a result, the magnetic pressure increases in these regions and causes an expansion of the poloidal field. This is seen most clearly in the bottom rows. Magnetic loops that connect the star to the disk "puff out" in the region above and below the disk. Plasma that is attached to these field lines moves with them. Thus the expansion drives an outflow. As the expansion drives some field lines toward the rotation axis, attached plasma will be driven outward along this axis. This outflow is seen more clearly in the top row.

A fast-mode MHD shock, the dominant feature in the temperature profile of the top row, separates the outflow from the ambient medium. Evidence that outflow is driven by the expansion of the field that threads the innermost edge of the disk is seen in the rapid separation of the shock from the field lines that are expanding through differential rotation. The fast-mode MHD shock crosses more slowly expanding field lines, those that thread the disk far from the star, as evidenced by the "kink" in those field lines above and below the disk. The outflow overtakes these more distant field lines before they themselves can inflate through differential rotation. This feature, which clearly demonstrates that the innermost regions of the threaded disk are most important in the development of the outflow, is also apparent in the results of Hayashi et al. (1996). The peak temperature of the shock is 2×10^6 K. The peak velocities shown in the last panel are 200 km s^{-1}, and the particle densities shown in gray-scale range from 10^{11} to $10^7\ \mathrm{cm}^{-3}$.

The fast-mode shock that forms around the head of the outflow is reminiscent of the bow shocks of Herbig-Haro objects. The strongest outflow is along the rotation axis and is produced by the convergence toward the rotation axis of plasma attached to expanding field lines. The shock is therefore strongest along the rotation axis. While the velocity profile decreases monotonically with increasing angle off-axis, the density begins to increase dramatically along the rotation axis and along the disk. This effect, which will be illustrated more clearly later, produces a two-component outflow in momentum.

The field configuration predicted by LRBK is obtained in the region close to the star, as shown in the last panel on the bottom row of Figure 5. As predicted by LRBK, high-latitude field lines on the star become effectively open, while field lines that thread the accretion disk are also effectively open but oppositely directed. A closed stellar magnetosphere exists close to the star. The open stellar field and open disk field do indeed ultimately connect, but only after extending out and around the expanded field region. The high-latitude stellar field and the disk field can be treated as effectively open, in that it is difficult to transfer magnetic stress from the star to the disk, and accretion can occur only by the diffusion of plasma across magnetic field lines. Magnetic reconnection, however, can change the field topology

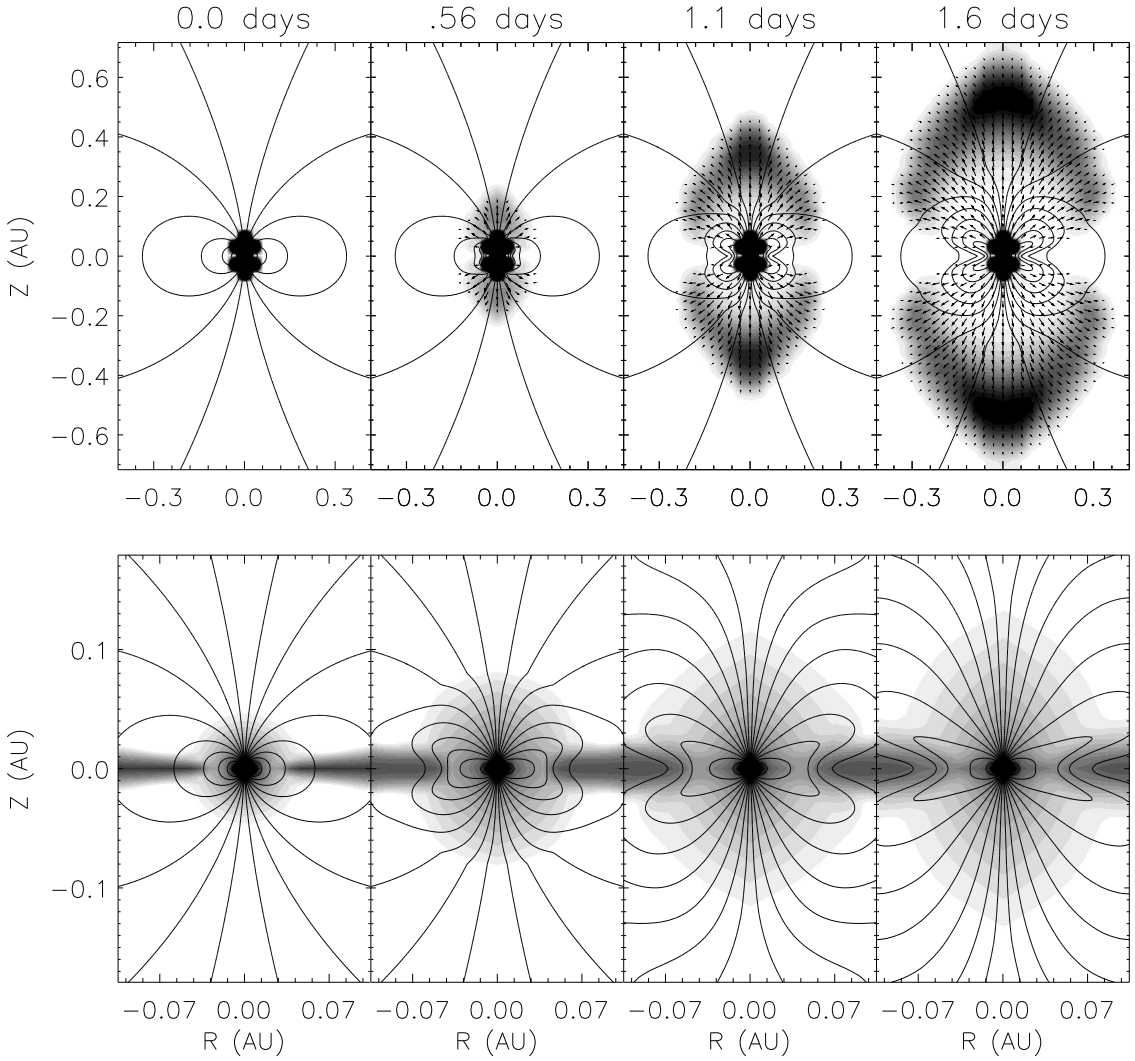

FIG. 5.—Early evolution of star/disk system. The top row shows temperature (gray scale), velocity and poloidal magnetic field lines. The toroidal field is not shown. The bottom row has 4 times the resolution of the top row, and shows $\log_{10} \rho$ (gray scale) and magnetic field lines. Differential rotation between the star and disk rapidly inflates the B field, initiating an outflow. The outflow is separated from the ambient plasma by a fast-mode MHD shock (seen in the top row).

so that the star is again connected to the disk, and plasma can flow along the newly connected field lines and onto the star. It should be noted that the environment shown at the end of the evolution in Figure 5 is a transient one. The disk is massive (when the kinetic energy density is compared to the magnetic energy density), and the inner edge of the disk is in the process of spiraling in close to the star.

The characteristics of the outflow to this point are strongly dependent on the initial density profile and assumed initial rotational velocity profile of the plasma above and below the disk. The outflow shown in Figure 5 consists of initial background plasma that was originally in the regions above and below the disk. In this sense, the outflow and the shock are initialization processes. Magnetic reconnection will sustain the flow, however, and generate an outflow that consists of disk plasma. This outflow of disk plasma does not depend on the initial distribution of plasma above and below the disk. As mentioned above, reconnection between the open disk field and the open stellar field will allow for accretion of disk plasma along these newly connected field lines, provided that the field lines connect the star to a point in the disk that is inside the Keplerian corotation radius. Thus if reconnection occurs, the accretion rate of plasma onto the star can be expected to be unsteady.

More important (with respect to the formation of stellar jets), reconnection between the open stellar field and open disk field will connect the star to the disk magnetically. If the star and the region of the disk to which it reconnects rotate with different angular velocities, the flux connecting the two will again inflate rapidly. Some disk plasma will have been loaded onto these field lines prior to the initiation of the expansive phase. The second expansion will drive an outflow of plasma that originated in the disk. The necessary condition for this outflow is reconnection in the region above and below the disk, with subsequent loading of field lines with disk plasma.

Figure 6 shows this reconnection event. $\mathrm{Log}_{10}(\rho)$ and magnetic field lines are shown in the figure. To highlight changes in B-field topology, many magnetic field lines are drawn. The initial B-field inflation is well underway by the first panel. The inner edge of the disk moves in toward the star between the first and second panels, dragging frozen-in flux with it. Noting that $\boldsymbol{J} \propto \nabla \times \boldsymbol{B}$, one can see that a strong current sheet exists above and below the accretion

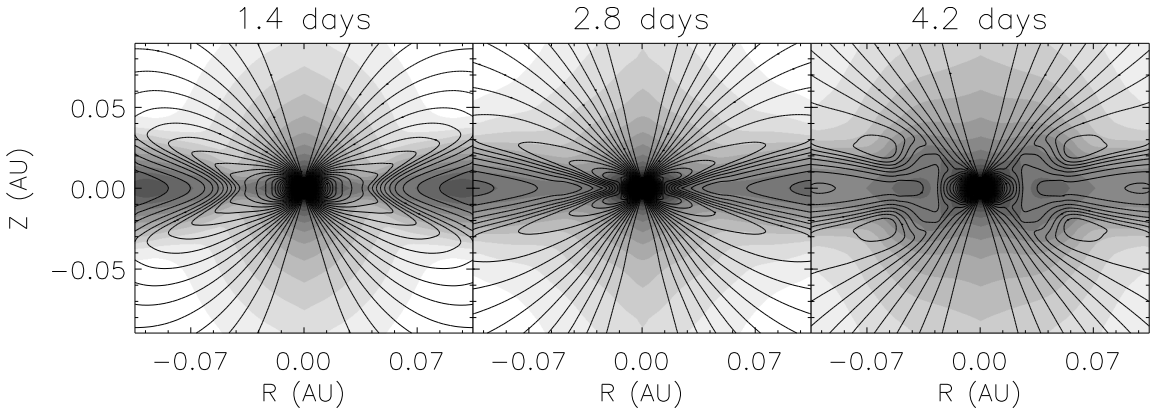

FIG. 6.—Evolution of $\log_{10} \rho$ and poloidal field for the region close to the star, with reconnection. The disk moves in toward the star between the first and second panels, with reconnection above and below the disk occurring between the second and third panels.

disk. This current sheet is disrupted between the second and third panels, and the resultant postreconnection field configuration is shown in the last panel. This reconnection frees a large plasmoid (much larger than the scale of the figure), but, more important, it reestablishes a near-dipolar field configuration that threads the disk and connects to the star. This closed field can be seen in the last panel of the figure. It should be noted that the disk plasma is now disrupted near the star (the disk has an increased scale height in density), but the disk still has a dense core. Differential rotation between the star and the disk can cause the magnetic field to expand rapidly again.

There are some local high-speed flows associated with the reconnection, and ohmic heating can produce very high temperatures. These events could likely be observed as X-ray flares, as pointed out in Hayashi et al. (1996). Hayashi et al. invoke a conservation of angular momentum argument to predict that the freed plasmoid should have a velocity vector that is eventually aligned with the rotation axis. Using this prediction, Hayashi et al. assume that the observed jet may actually be optical emissions from the hot, low-density cores of the plasmoids. (In this picture, the jet would really be a series of doughnut-shaped hot toroids moving in the same direction.) While the results to be presented below show that the plasmoids do eventually collimate (although the driving mechanism appears to be containment by the disk boundary), the jets to be shown in this paper are actually not the plasmoids but the cooler plasma driven toward the axis during the plasmoid formation process. While reconnection can produce local flows with speeds of order of the Alfvén speed, which also happens to be about 200 km s^{-1} for this simulation, the primary large-scale effect of reconnection appears to be the initiation of subsequent outflow-generating expansions.

Hayashi et al. (1996) produce plasmoids that are qualitatively similar to the ones produced in this work but that have a somewhat different shape and temperature profile. The main difference arises from the treatment of resistivity. Hayashi et al. have an explicit resistivity that is proportional to the square of the current, i.e., $\eta = 1/\sigma = \eta_0(v - v_{co})^2$, where $v = |J|/\rho$ and v_{co} is a cutoff value. When the local current magnitude is greater than ρv_{co}, then the resistivity is set by the above equation. When the local current magnitude is less than ρv_{co}, then the resistivity is set to zero. The result of this treatment of resistivity is the increase of the reconnection rate (once reconnection is triggered) and of ohmic heating. By examining equations (3) and (6) in conjunction with this resistivity, one can see that ohmic heating in the Hayashi model is proportional to $|J|^4$. Thus, one would expect the plasmoids in the work of Hayashi et al. to be released earlier than those of this work (and therefore to be smaller), and to have a much hotter plasma generated in the reconnection region, which is consistent with the differences between the results.

A second-order difference between these results and those of Hayashi et al. is related to the rotating star. The star in this work is rotating with a period of 1.8 days, while Hayashi et al. have a nonrotating star. The rapidly rotating star flings the plasmoids out with an opening angle of approximately 145° (for the region very close to the star), while the nonrotating star of Hayashi et al. produces an opening angle of approximately 100°. It should also be noted that Hayashi et al. are limited by the size of the simulation box used. The nested box scheme used for this work decreases box-size limitations for these results.

The initiation of the second expansion is shown in Figure 7. The time corresponding to the first frame of Figure 7 is identical to that in the last frame of Figure 6, but the data are shown at twice the resolution. After the stellar field has reconnected with the disk, differential rotation between the star and the disk leads to the same inflation process as described earlier. The first panel shows the field configuration after reconnection. The second panel shows an expansion beginning in the region very close to the star, and the third panel shows the more well-developed inflation. This expansion will continue to drive outward until it too is freed through reconnection at its base.

The large-scale, long-term behavior of the flow is shown in Figure 8. The bottom row shows $\log_{10}$(density) in gray scale and has 4 times the resolution of the top panel, which shows temperature in gray scale. The formation of the first and second sets of plasmoids proceeds as described above in the previous figures. Reconnection above and below the disk frees the first plasmoid, and subsequent differential rotation between the star and the disk leads to the expansion and generation of a second plasmoid. The plasmoids become "finger shaped" as they grow. Note the distant removal of the shock from the expansion region for later times. The peak flow speeds for the later times in the figure are about 250 km s^{-1}. At the last panel, a third expansion

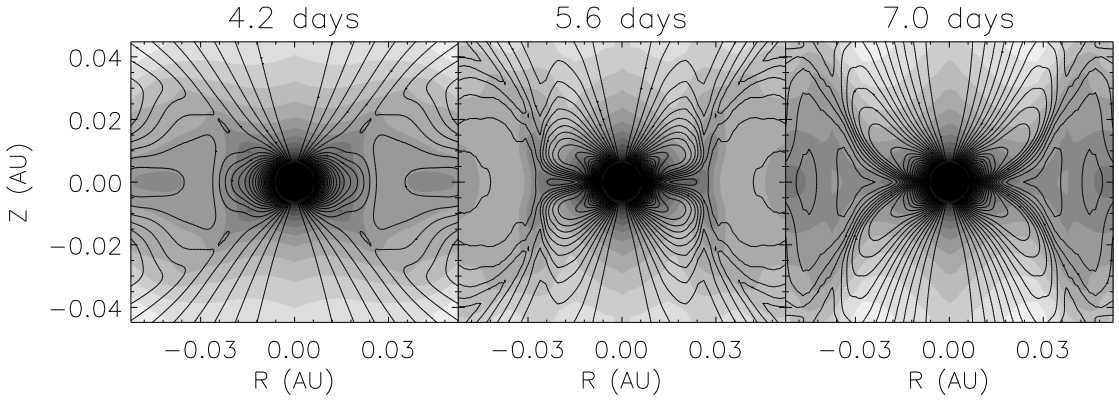

FIG. 7.—Initiation of second inflation phase. Stellar field threads disk after reconnection, and the region to which the star is magnetically connected rotates at a different rate than the star. The second panel shows initiation of expansion very close to the star, while the third panel shows the expansion in progress.

has commenced in the region very close to the star but is not visible with the resolution afforded by the figure.

Toward the end of the evolution shown in the bottom row of Figure 8, a significant amount of plasma has been driven toward the rotation axis. This can be seen in gray scale. Furthermore, stellar flux that threads the disk close to the star has been laid down along the surface of the disk. It is this flux (the effectively open disk field) that is predicted

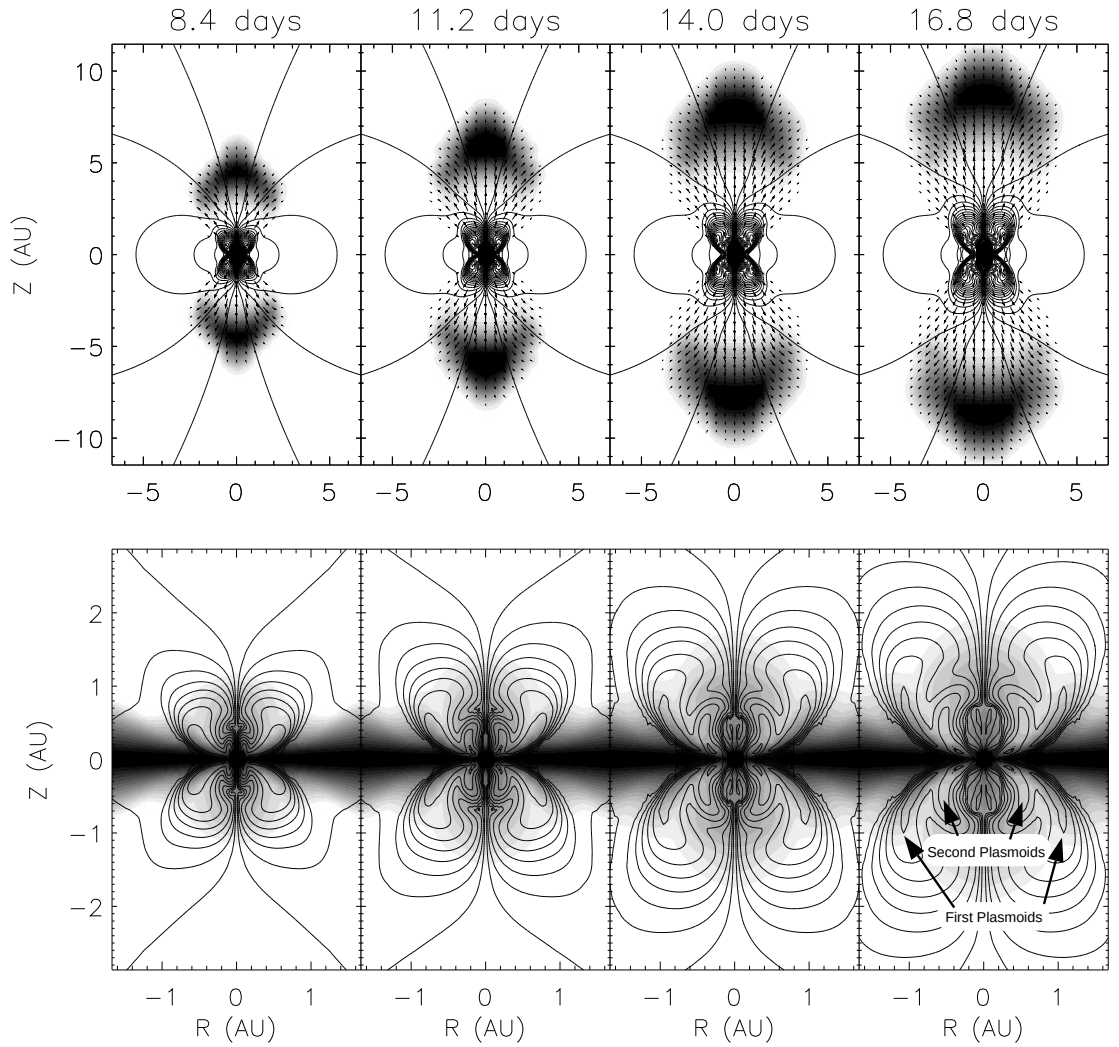

FIG. 8.—Large-scale evolution of star/disk system through the formation of the second set of plasmoids. In the top row, the outflow produced by the field expansion close to the star has a peak velocity of about 250 km s^{-1}, which produces a fast-mode Alfvén shock. The shock is smeared by the coarse resolution of the simulation in this region.

by LRBK to drive an outflow. Indeed, the outflow produced in this region, which is driven in part centrifugally, is a disk wind. It should also be noted that since the plasmoids drive flux against the surface of the disk, a density gradient is created that is steeper than that predicted for a disk driven by only gravitational, thermal, and viscous forces.

Figure 9 shows the two-component outflow. Velocity is shown only where the density is above a threshold value. The magnitude of the velocity field decreases monotonically with increasing angle off-axis, but the momentum would show a distinct two-component outflow. Similarly, observations that depend on the density of plasma would show a two-component outflow. The central jet, which is highly collimated and fairly hot, is driven by the convergent flow of plasma toward the rotation axis (which is produced by the series of field inflation episodes). The poorly collimated outflow that skims along the surface of the disk is the "disk wind." This flow is driven both by the expansion of the poloidal field and by the centrifugal flinging of plasma. As the field lines that thread this region of the flow are footed in the disk close to the star, plasma can be flung outward like beads on a wire. Blandford & Payne (1982) have shown that if the initial tilt angle of the field line is more than 60°, then the field line will "point downhill," in terms of the effective potential (the gravitational potential in the rotating frame). Plasma can thus be flung centrifugally. The plasmoids occupy the region of low density that surrounds the jet and separate the jet from the disk wind.

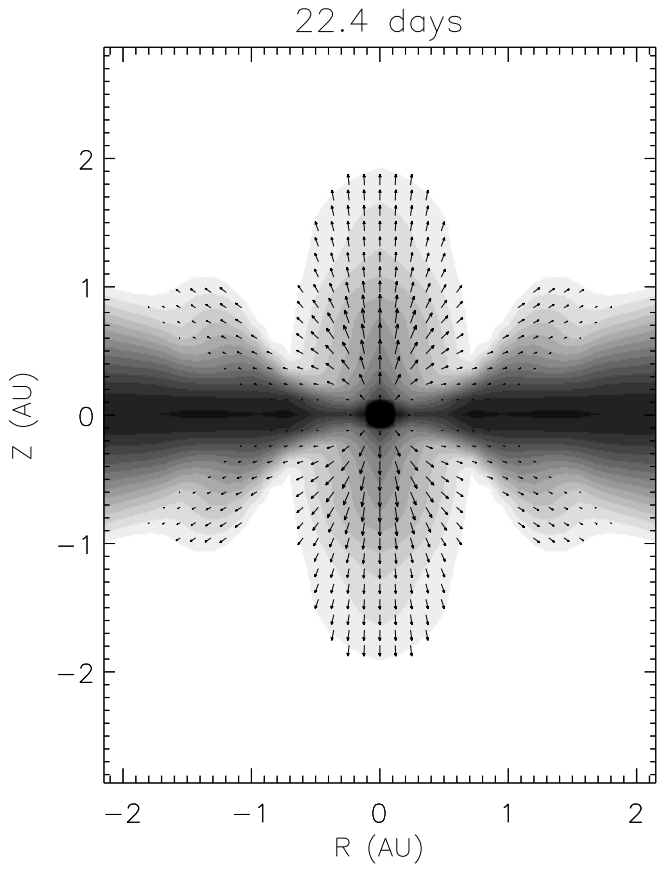

FIG. 9.—Two-component outflow. $\mathrm{Log}_{10}\,\rho$ (with a range of 4 orders of magnitude) and velocity are shown. Velocity is not shown when density is below the (arbitrary) cutoff value. A collimated jetlike outflow is clearly seen, as is a "disk wind." The plasmoids lie in the region that separates the two outflow components. The concentration of flux and plasma toward the rotation axis produces a well-collimated (hot) outflow, while the concentration of flux and plasma toward the disk produces a poorly collimated, cooler, slower outflow. The collimated outflow could be the jet, and the poorly collimated flow could be the disk wind. The "disk wind" is driven centrifugally, in part.

The disk wind has typical poloidal velocities of 40–80 km s^{-1}, is launched in a cone with an approximately 140° opening angle, and has a rotational component (at the point shown in Fig. 9) of about 10 km s^{-1}. If observations were made of this system from a distant point along the rotation axis, one would expect to see a velocity spectrum qualitatively similar to that of DG Tau (see Solf & Böhm 1993). The mass-weighted velocity spectrum of the simulated outflow shows a jet with a high-velocity component (roughly 200 km s^{-1} in this case) and relatively low dispersion (30–50 km s^{-1}), accompanied by the disk wind, which has a centroid velocity of 15 km s^{-1} and comparable dispersion. Should the observer be off axis, the jet's centroid velocity would decrease (but its dispersion would not). As the disk wind has such a large opening angle, off-axis observers would see a large velocity dispersion in the disk-wind component.

Figure 10 shows the time evolution of the jet structures in the same general format as Figure 9. The jet grows over time in both length and width but, in general, grows faster in length. The aspect ratio of the entire jet (end to end) changes from about 2.4 in the first frame to about 4.0 in the last frame, although some oscillation in aspect ratio occurs. The disk-wind region also grows, with a distinct wave front separating the leading edge of the disk wind from the ambient plasma. This wave front is on the edge of the image for the third frame of the figure, and off the image for the last frame.

As mentioned above, the disk wind is in part centrifugally supported. Figure 11 shows the torque on the plasma resulting from the magnetic force term, i.e., $\boldsymbol{r} \times (\boldsymbol{J} \times \boldsymbol{B})$. The region shown is fairly close to the star, and the torques within 1.5 stellar radii of the central star are not shown. The cube root of the torque is plotted, with negative torques shown as dashed lines and positive torques as solid lines. At the time of the figure, the disk is truncated within one stellar radius of the star. As seen in the figure, significant acceleration in the $+\phi$ direction is generated by the magnetic field in the regions above and below the disk. This is consistent with the predictions of LRBK with respect to disk winds. Additionally, one can see that there is a significant back torque on the core of the disk itself, which can be very effective at removing angular momentum. As the system is examined at larger and larger radii (much larger than that shown in this figure), one finds that the torque on the disk is concentrated at the disk surface. This transient effect results from the frozen-in flux approximation holding (to first order) in the disk itself; thus the field in the disk only slowly evolves from the initial (force-free) dipole field, while the field at the surface of the disk rapidly departs from the force-free condition because of the quick change of the field in the region above and below the disk.

In summary, this work shows that the rapid inflation of the B field can lead to the formation of a two-component outflow: a fast, hot, well-collimated outflow along the rotation axis (a jet) and a slower, cooler, poorly collimated outflow near the surface of the disk. The jet and disk wind are separated by plasmoids formed by the rapid inflation process. This time-dependent view produces a sustained jet

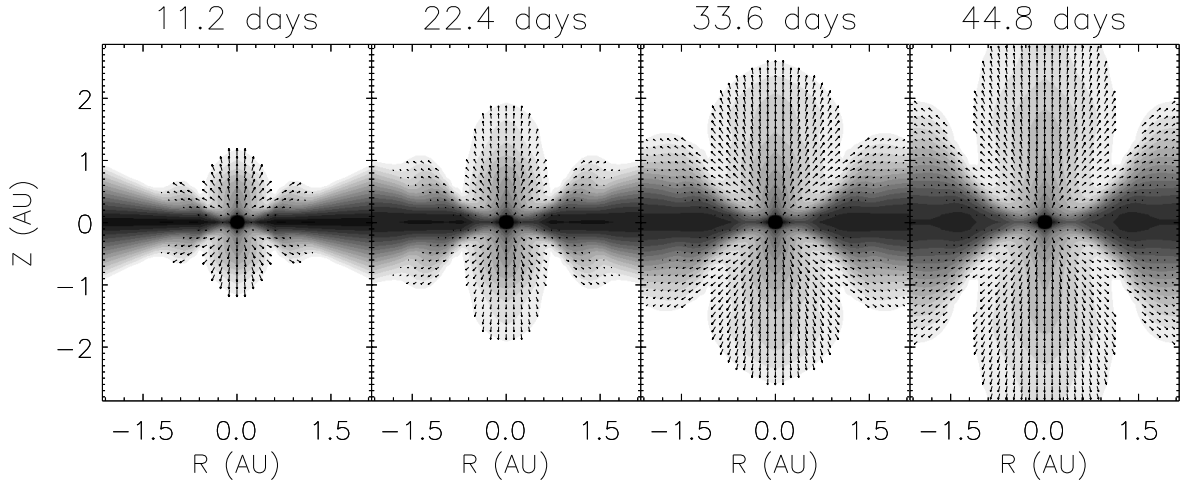

FIG. 10.—Evolution of two-component outflow

only under the condition of multiple sequential inflation episodes. These are achieved through magnetic reconnection above and below the disk plane.

5. DISCUSSION

The results presented here show promise for understanding the mechanism that launches stellar jets. A single model has produced an outflow that compares favorably with observations and has two components: a jetlike, highly collimated, fast outflow and a poorly collimated, slow outflow reminiscent of a disk wind. The physical process that produces the outflow depends on differential rotation between the star and the portion of the accretion disk to which it is magnetically connected, and the jet is maintained through magnetic reconnection. The most important new ideas introduced in this work are that (1) the *time-dependent* inflation of the *B* field produces an outflow, and (2) the outflow is sustained by repeating the inflation process, i.e., through reconnection. The outflows shown can develop only in a time-dependent way.

There are five necessary conditions required for this mechanism to generate an outflow from a YSO:

1. The star must be magnetically connected to a region of the surrounding accretion disk.
2. The region to which the star is connected must rotate with a different angular velocity than the star.
3. The region of the disk must have conductivity that is high enough to support the frozen-in flux approximation. This condition may be attainable via photoionization at the disk truncation point as well as through ionization by the large X-ray flux expected from reconnection events.
4. Reconnection must occur in the region above and below the disk.
5. The newly connected field lines must become loaded with disk plasma before a subsequent expansion occurs.

Any system that meets the first three conditions must undergo a period of rapid expansion of the *B* field. The existence of this expansion episode has been demonstrated by other researchers (LRBK; Zylstra 1988; Aly & Kuijpers

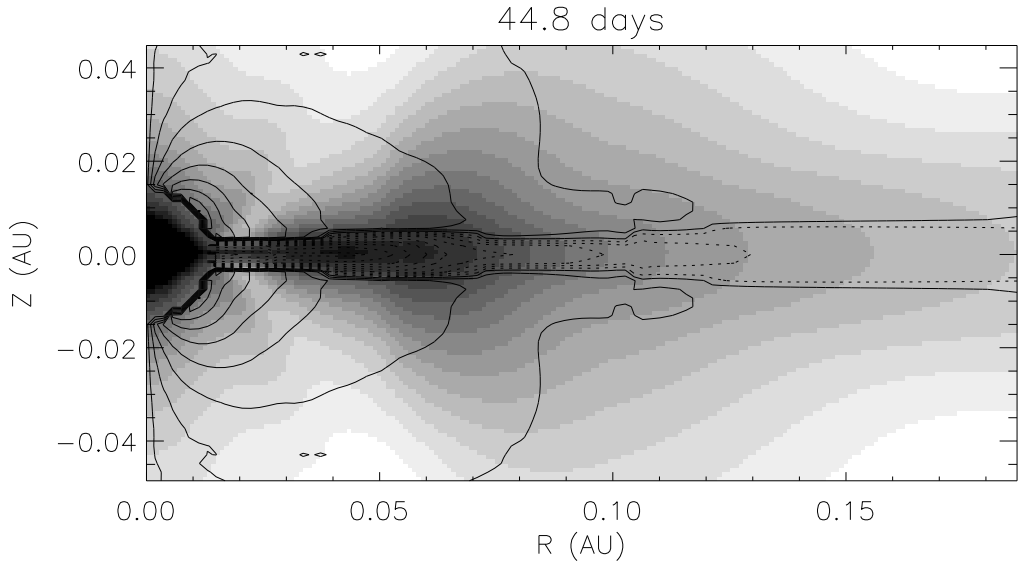

FIG. 11.—Magnetic torque [$r \times (J \times B)$] in the region of well-developed outflow. The disk wind is in part centrifugally supported (positive torque), while the disk itself is torqued down.

1990). Most past workers go on to address the steady state implications of this configuration, assuming that no reconnection occurs between the open stellar field and the open disk field. If no reconnection occurs, the field configuration remains as predicted by LRBK or assumed a priori by Shu et al. (1994a).

Reconnection between the open stellar field and the open disk field again connects the star with a conducting region of the disk that rotates at a different angular rate. Thus, reconnection allows for multiple episodic expansion phases. Hayashi et al. (1996) have examined a single postexpansion reconnection event and the plasmoid that is formed. They state that such plasmoids may eventually collimate, because of angular momentum conservation, but cannot demonstrate this collimation, because of the constraint of the simulation box size. The work presented here implies that the plasmoids are not the jet, as suggested by Hayashi et al., but rather serve to separate the jet from the disk wind.

Each expansion phase will drive attached plasma toward the rotation axis (to form a jet) or toward the disk (to form a disk wind). Should the expanding field lines be loaded with disk plasma prior to the expansion of the B field (the last of the necessary conditions), then the jet will consist of plasma that originated in the disk. For this condition to be met, field-aligned accretion must occur from the newly connected region of the disk. This implies that this region must be inside the centrifugal barrier.

While the current results show a smooth outflow, an increase in the time interval between expansion phases may produce a jetlike outflow that consists of a series of "interstellar bullets" of plasma. Ongoing work is addressing the influence of the spatially uniform resistivity over the frequency of the expansion phases. Further investigations will attempt to establish the long-term evolution of the system, with sensitivity to stellar rotation rate, disk density, and field strength, and an attempt will be made to compare results of highly evolved systems directly with observations.

This work begins with the assumption that the stellar dipole field threads the accretion disk out to all $\bar{\omega}$. While the mechanism at work requires that the disk be threaded by the magnetic field at a location that has a different angular velocity than the star, these results indicate that it is not critical that the entire disk be threaded. Indeed, the innermost edge of the disk seems to be the most critical. Thus if stellar flux threads the disk only at the innermost edge, and there is differential rotation between the star and the inner disk with a period several times less than the local diffusion time, the mechanism presented here should produce a jet.

A disk that excludes the magnetic field in all places except for a small region at its innermost edge—such as that assumed by Shu et al. (1994a), but with the constraint of placement at the corotation radius removed—should thus be well suited for the production of jets. If the stellar magnetic field for YSOs develops after the disk is established, then the inner edge of the disk may be pushed back from the star, and the field may be mixed in with the disk's inner edge. That done, the jet formation process could commence. An explanation for stellar jets could thus be at hand.

The authors would like to thank Frederick K. Lamb for his help early in this effort. This work was supported by the University of Washington Royalty Research grant 65-2597 and NSF grant ATM-9321665

REFERENCES

Aly, J. J., & Kuijpers, J. 1990, A&A, 227, 473
Blandford, R. D., & Payne, D. G. 1982, MNRAS, 199, 883
Böhm, K. H., & Solf, J. 1994, ApJ, 430, 277
Cameron, M., & Liseau, R. 1990, A&A, 240, 409
Edwards, S., Ray, T., & Mundt, R. 1993, in Protostars and Planets III, ed. E. H. Levy & J. I. Lunine (Tucson: Univ. Arizona Press), 567
Eisloeffel, J., Mundt, R., & Böhm, K. H. 1994, AJ, 108, 1042
Elsen, R. K., & Winglee, R. M. 1997, J. Geophys. Res., A102, 4799
Feigelson, E. D., Casanova, S., Montmerle, T., & Guibert, J. 1993, ApJ, 416, 623
Frank, J., King, A., & Raine, D. 1992, Accretion Power in Astrophysics (Cambridge: Cambridge Univ. Press)
Frank, A., & Mellema G. 1996, ApJ, 472, 684
Fukui, Y., Iwata, T., Mizuno, A., Bally, J., & Lane, A. P. 1993, in Protostars and Planets III, ed. E. H. Levy & J. I. Lunine (Tucson: Univ. Arizona Press), 603
Ghosh, P., & Lamb, F. K. 1978, ApJ, 223, L83
———. 1979a, ApJ, 232, 259
———. 1979b, ApJ, 234, 182
Guenther, E. W. 1997, in IAU Symp. 182, Herbig-Haro Flows and the Birth of Low-Mass Stars, ed. B. Reipurth & C. Bertout (Dordrecht: Kluwer), in press
Hartigan, P., Raymond, J., & Hartmann, L. 1987, ApJ, 316, 323
Hartmann, L., & Raymond, J. 1984, ApJ, 276, 560
Hayashi, M. R., Shibata, K., & Matsumoto, R. 1996, ApJ, 468, L37
Herbig, G. H. 1951, ApJ, 113, 697
———. 1981, AJ, 86, 1232
Hirth, G. A. 1994, in ASP Conf. Ser. 57, Stellar and Circumstellar Astrophysics, ed. G. Wallerstein & A. Noriega-Crespo (San Francisco: ASP), 32
Hirth, G. A., Mundt, R., & Solf, J. 1994, A&A, 285, 929
Kepner, J., Hartigan, P., Yang, C., & Strom, S. 1993, ApJ, 415, L119
Königl, A. 1982, ApJ, 261, 115
Königl, A., & Ruden, S. P. 1993, in Protostars and Planets III, ed. E. H. Levy & J. I. Lunine (Tucson: Univ. Arizona Press), 641
Koyama, K., Maeda, Y., Ozaki, M., Ueno, S., Kamata, Y., Tawara, Y., Skinner, S., & Yamauchi, S. 1994, PASJ, 46, L125
Kwan, J., & Tademaru, E. 1988, ApJ, 332, L41
Lovelace, R. V. E., Romanova, M. M., & Bisnovatyi-Kogan, G. S. 1995, MNRAS, 275, 244
Mundt, R. 1985, in Protostars and Planets II, ed. D. Black & M. S. Mathews (Tucson: Univ. Arizona Press), 414
Najita, J., & Shu, F. 1994, ApJ, 429, 808
O'Dell, C. R., & Wen, Z. 1994, ApJ, 436, 194
Raga, A. C. 1989, in ESO Conf. Ser. 33, Low Mass Star Formation and Pre–Main Sequence Objects, ed. B. Reipurth (Garching: ESO), 281
Raga, A. C., & Böhm, K. H. 1986, ApJ, 308, 829
Raga, A. C., & Cantó, J., 1989, ApJ, 344, 404
Raga, A. C., & Kofman, L. 1992, ApJ, 386, 222
Ray, T. R., Mundt, R., Dyson, J. E., Falle, S. A. E. G., & Raga, A. C. 1996, ApJ, 468, L103
Ray, T. P., Muxlow, T. W. B, Axon, D. J., Brown, A., Corcoran, K., Dison, J., & Mundt, R. 1997, Nature, 385, 415
Reipurth, B. 1991, in Physics of Star Formation and Early Stellar Evolution, Proc. NATO Adv. Study Inst., ed. C. L. Lada & N. D. Kylafis (Dordrecht: Kluwer), 497
Reipurth, B. 1994, General Catalogue of Herbig-Haro Objects (Paris: ESO)
Richtmyer, R. D., & Morton, K. W. 1967, Difference Methods for Initial-Value Problems (New York: Wiley-Interscience)
Shibata, K., & Uchida, Y. 1986, PASJ, 38, 631
Shu, F., Najita, J., Ostriker, E., Wilken, F., Ruden, S., & Lizano, S. 1994a, ApJ, 429, 781
Shu, F., Najita, J., Ruden, S., & Lizano, S. 1994b, ApJ, 429, 797
Solf, J. 1989, in ESO Conf. Ser. 33, Low Mass Star Formation and Pre–Main Sequence Objects, ed. B. Reipurth (Garching: ESO), 399
Solf, J., & Böhm, K. H. 1993, ApJ, 410, L31
Uchida, Y., & Shibata, K. 1985, PASJ, 37, 515
Zylstra, G. 1988, Ph.D. thesis, Univ. Illinois at Urbana-Champaign